Engineering Structures 134 (2017) 37–47

Contents lists available at ScienceDirect

Engineering Structures

journal homepage: www.elsevier.com/locate/engstruct

Global sensitivity analysis of lateral-torsional buckling resistance based on finite element simulations

Zdeněk Kala *, Jan Valeš

Brno University of Technology, Faculty of Civil Engineering, Department of Structural Mechanics, Veveri Street 95, 602 00 Brno, Czech Republic

ARTICLE INFO

Article history:
Received 10 August 2016
Revised 22 November 2016
Accepted 19 December 2016

Keywords:
Sensitivity analysis
Stability
Reliability
Lateral-torsional buckling
Steel
Beam
Imperfections
Out-of-straightness
Residual stress
FE modelling

ABSTRACT

The article examines a hot-rolled steel I-beam subjected to lateral-torsional buckling (LTB) due to bending moment. The paper describes a non-linear finite element (FE) model and numerical approximation and simulation methods used for the global sensitivity analysis of the static resistance of a beam under major axis bending. The presented geometrically and materially non-linear FE model based on solid elements models in detail the LTB and the effects of initial imperfections on the ultimate limit state of a steel beam. Simulation runs of random imperfections are generated using the Latin Hypercube Sampling (LHS) method. Polynomial approximation of the model output helped minimise the number of runs of the non-linear finite element model. The approximation polynomial then facilitated the evaluation of sensitivity indices using a high number of simulation runs. The relationships between the slenderness and the first and second-order sensitivity indices are plotted in graphs. The graphs show the results of global sensitivity analyses of stochastic effects of initial imperfections and residual stress on the resistance of the investigated steel beam.

1. Introduction

Lateral-torsional buckling (LTB) is a typical failure mode of unbraced I-beams subjected to bending about the major principal axis that both twist and deflect laterally. Lateral-torsional buckling resistance (LTB-R) including the effects of imperfections, residual stresses and plasticity effects may exhibit broad stochastic scattering due to the random influence of these effects [1]. Detrimental imperfections like initial curvature of the axis and residual stress may dramatically reduce the LTB-R. High sensitivity of LTB-R to the stochastic variability of initial imperfections increases the probability of failure of beams. Due to these reasons, it is important to study the effects of these inevitable initial imperfections and residual stresses on the LTB-R, which is the goal of the presented article.

The research of thin-walled beams has evolved from the classic Vlasov theory [2] to advanced non-linear finite element (FE) models; see e.g. [3–8]. In literature, the imperfect I-beam subjected to uniform bending moment is the only case for which the elastic closed-form analytical solution of lateral-torsional buckling resistance (LTB-E) exists [9]. The development of numerical methods, such as FE methods, has lead to the continuous investigation of the available closed form solutions present in standard literature [9–13] and codes [14–16]. It has been clearly shown that such formulae are often conservative and in certain cases wrong [17].

The efficient use of computational models requires an understanding of key relationships between inputs and outputs. Analytical, especially numerical models of LTB failure modes are unfortunately often so complex that they prevent the understanding of the response of the model output to changes in model inputs based on intuition.

The dependence of model output on model inputs can be studied using stochastic sensitivity analysis (SA). The diversity of problems that are solved using mathematical modelling has recently lead to the development of several highly successful methods of sensitivity analysis [18–21]. Advanced methods of stochastic global sensitivity analysis are usually highly numerically demanding, especially in cases where it is necessary to evaluate the sensitivity indices using the Monte Carlo numerical simulation method. The computer time needed for the evaluation of one realization (one run) of the output random variable increases with increasing complexity of the computational model. Furthermore, the more complex the sensitivity analysis, the more realizations (numerical simulations) are needed to obtain statistically correct output.

* Corresponding author.
E-mail addresses: kala.z@fce.vutbr.cz (Z. Kala), vales.j@fce.vutbr.cz (J. Vales).

http://dx.doi.org/10.1016/j.engstruct.2016.12.032
0141-0296/

In engineering fields, scientists try to keep up to date with the current trends of modern research aimed at global sensitivity analysis (GSA) of model outputs [22]. GSA is necessary in situations where a priori information on the nature of the model is unavailable (model-free setting) or the model is considered to be non-additive [23]. In contrast, local SA (LSA) puts emphasis on the local (point) impact of the input factors on the model output [20]. LSA, which is also known as differential SA, belongs to the class of the one-factor-at-a-time methods. LSA has apparent advantages [21]. It is very straightforward compared to GSA, thus, making it easy to apply and interpret. In the case of a linear model, all information needed for SA is obtained from the first-order derivatives [24]. In the case of a non-linear but additive model, i.e. no interactions are present among factors, then derivatives of higher and cross order suffice to understand the model [24]. LSA cannot be used to describe higher-order interaction effects among factors. The outputs of non-linear and non-monotonous computational models such as LTB-R should be studied with GSA. One of the most effective methods of stochastic GSA is Sobol's sensitivity analysis SSA [25,26], which is based on the total decomposition of the variance of the output variable into terms with increasing dimensions.

In this article, SSA is used to map the influence of random input imperfections on the ultimate (inelastic) lateral-torsional buckling resistance (ultimate load carrying capacity) denoted as LTB-R. The term imperfection refers collectively here to both geometrical (initial axial twist and curvature, tolerance of dimensions of the cross section) and material (yield strength, residual stress, Young's modulus) imperfection [27]. The stochastic LTB-R was evaluated by Monte Carlo runs using Latin hypercube sampling (LHS) [28,29] on I-beam samples, which are randomly generated and subsequently analysed using the commercially available geometrically and materially non-linear FE program ANSYS [30].

A highly detailed model based on non-linear FE method allows detailed modelling of the effects of all imperfections on LTB-R. End-fork boundary conditions and uniform bending moment loading were considered, see Fig. 1. An elastic solution in the closed form [9], which was applied for the evaluation of LTB-E (lateral-torsional buckling resistance including the effects of imperfections, without residual stress and based on elastic and first yield analysis) [31,32], also exists for this type of boundary condition and loading. SSA was evaluated for LTB-R and LTB-E and the obtained results were compared. Due to the high complexity of the repeated calculations of LTB-R, SSA of the FE model was not performed, but rather the SSA of the polynomial approximation of the FE model.

2. FE model

Numerical simulations were performed using the Ansys software [30] as a process of running geometrically and materially non-linear model with regard to imperfections, such as initial geometric imperfections and residual stresses. The FE research was performed on a model of European hot-rolled steel I200 beam, which is statically loaded on both ends by bending moment M, see Fig. 1.

Due to potential problems that could occur whilst generating the FE mesh, the cross-sectional geometry of I200 was slightly simplified and fillets in the flange-to-web connection and at the ends of the flanges were neglected. The cross-sectional geometry of I200 is considered as biaxially symmetrical. The I200 cross-section is thus defined by five dimensions h, b, t_1, t_2 and α, see Fig. 2. According to [33], the effect of the fillet was found to be negligible in LTB problems.

Commercially available software ANSYS was used for the FE analysis. Homogeneous structural solid element SOLID185 was used for the model. It is an 8-node element having three degrees of freedom at each node: translations in the nodal x, y, and z directions. It is suitable for 3D modelling of solid structures. It has plasticity, hyper-elasticity, large deflection and large strain capabilities, stress stiffening and creep. The enhanced strain formulation, which prevents shear locking in bending-dominated problems and volumetric locking in nearly incompressible cases, was considered. The element introduces nine internal degrees of freedom to handle shear locking, and four internal degrees of freedom to handle volumetric locking. All internal degrees of freedom are introduced automatically at the element level and condensed out during the solution phase of the analysis [30]. SOLID185 allows for prism, tetrahedral, and pyramid degenerations when used in irregular regions. However, this was not the case, and only hexahedron elements were created [30].

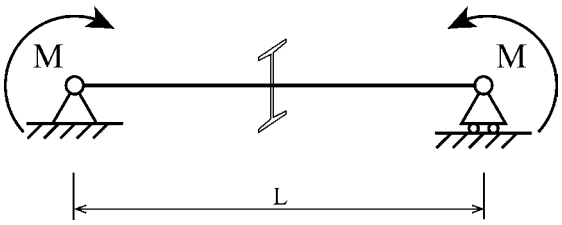

Fig. 1. Simply supported I-beam subjected to uniform bending moment.

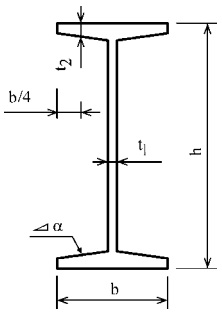

Fig. 2. The geometry of beam I200.

Even though it is customary to model LTB problems using shell elements instead of solid elements, certain undesirable effects, such as small material overlap in the flange-to-web connection, occur in shell models. The beam is thus a little bit more rigid and has a higher load-carrying capacity [3,34]. Another disadvantage of shell elements is the problematic modelling of the varying thickness of parts of the cross-section. In this case the flange thickness t_2. These undesirable effects were eliminated using solid elements SOLID185, however, at the cost of increasing demands on CPU time.

2.1. Mesh, boundary conditions and loads

Generally, the results obtained from the FE model are more accurate the finer the FE mesh. This, however, leads to an increase in the computational time. It is thus necessary to find a balance between the computational time and the desired accuracy. The mesh density was tested and the optimal setting of 20 elements over the entire height of the web, 10 elements over the entire width of the flanges and two elements over the web and flange thickness was chosen, see Fig. 3. It was tested that two elements over the thickness are sufficient and the final value of resistance is not influenced by the number of elements even in the plastic behaviour. The x–axis corresponds to the longitudinal axis of the beam; axes y and z lie in the plane of the cross-section. The origin of the coordinate system is placed in the centre of gravity of the cross-section. This also corresponds to the shear centre in a doubly

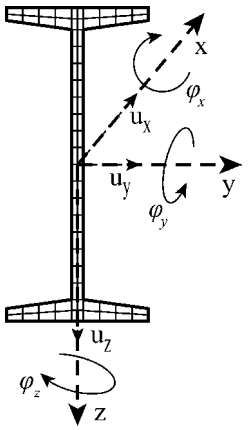

Fig. 3. The meshing of the cross-section I200.

symmetric cross-section. Translations u_x, u_y, u_z and rotations φ_x, φ_y, φ_z are related to the global coordinate system. The number of elements per length was selected in a manner such that the maximum ratio of the longest to shortest side of the element (maxrat) was equal to 8. It may be noted that, according to [30], the aspect ratio for quadrilaterals should not exceed 20. Otherwise disturbance of analysis results may occur. This implies that the number of elements per beam length is not constant and the number of elements increases with increasing length of the beam. Control calculations were performed for a finer mesh with 4 elements over the thickness and maxrat = 4. The finer mesh yielded slightly more accurate results (difference of several tenths of a percent) for beams with low slenderness. However, the results from the present denser mesh are due to the small difference acceptable. For slender beams the results with the finer mesh were practically identical. For beams with $\bar{\lambda}_{LT} = 2.0$ the accuracy of the FE model was also verified using the analytical solution in the closed form [31,32].

End-fork boundary conditions were considered for the model. These conditions make it possible to compare the elastic FE solution with the analytic solution [31,32] and verify the correctness of the model. Support conditions were created on both ends of the beam using three kinematic coupling constraints: two for the edges of the flanges and one for the axis of the web, see Fig. 4. Rotations φ_z and φ_y for the selected nodes of the web and flange respectively remain constant during loading, so that they are constrained to remain in a straight line. These boundary conditions were taken from the model presented in [3,34] and their implementation is crucial for the modelling of beams using solid or shell elements. Using these kinematic coupling constraints it is possible to overcome the occurrence of local extremes of stress at the end sections during loading and certain convergence problems of the calculation. Alternatively, instead of using these constraints, it is possible in the end sections to model zones with gradually increasing values of kinematic hardening of the material diagram of steel towards the edges [35]. However, this approach is not as effective.

A symmetric model was considered. Longitudinal translation of a point in the centre of gravity was constrained to $u_x = 0$ midspan of the beam. Boundary conditions of both ends of the beam are introduced into the centre of gravity and given as $u_y = u_z = \varphi_x = 0$, see Fig. 5.

The beam is loaded on both ends by equal bending moments M. Moments are applied as surface loads in the form of pressure p [N/m^2], which is defined by a gradient. The magnitude of the gradient is determined by the slope value (load per unit length) given as the ratio of the moment M to the moment of inertia I_y, and the distance from the z-axis, which represents the slope direction. The pressure acting on the element is given by the relationship $p = M \cdot z / I_y$. The pressure distribution is schematically shown in Fig. 5.

LTB-R was evaluated using the geometrically and materially non-linear FE method. The bending moment loading M was increased in steps until the value of $M_{LTB\text{-}R}$, where $M_{LTB\text{-}R}$ is the maximum bending moment loading corresponding to the ultimate limit state. $M_{LTB\text{-}R}$ is theoretically determined as the maximum moment M for which the determinant of the tangential stiffness matrix is equal to zero. Numerically, $M_{LTB\text{-}R}$ is determined as the moment in the last loading step for which the determinant of the stiffness matrix is very close to zero whilst the calculation is still converging. The steps of the loading moment $M_{LTB\text{-}R}$ are decreased so that the output value $M_{LTB\text{-}R}$ is calculated with an accuracy of 0.3%).

2.2. Material model

The material stress–strain curves of structural steels are investigated and discussed in [34]. Steel of grade S235 was selected for the numerical study performed in this article. The hardening slope of $E/10000$ was applied. The application of this hardening slope is based on a combination of numerical experience and recommendations of standards [36]. Annex C of [36] recommends the application of one of these four material behaviour models for plated FE analysis: (i) elastic–plastic without strain hardening, (ii) elastic–plastic with a nominal plateau slope of 1 MPa (or similarly small value), (iii) elastic–plastic with a strain hardening slope of $E/100$, (iv) true stress–strain curve modified from test results. The numerical instability of the FE computational model increases with

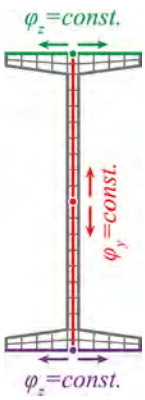

Fig. 4. Three kinematic coupling constraints.

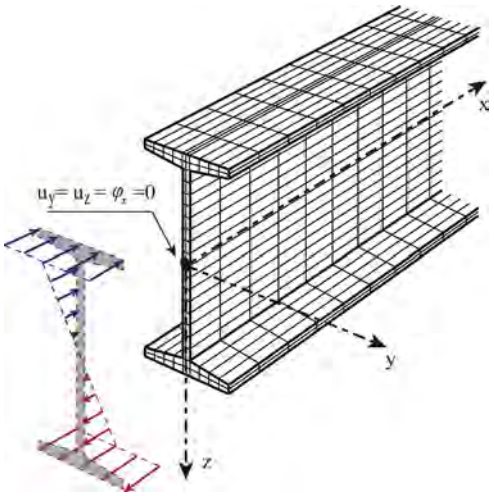

Fig. 5. The end-fork boundary conditions and equal bending moments.

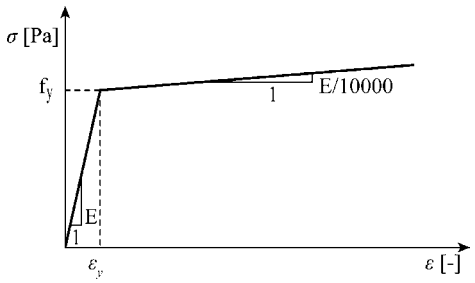

Fig. 6. Elastic-plastic stress-strain diagram of steel grade S235.

decreasing hardening slope, for e.g., the use of (i) lead to higher numerical instability than 1 MPa according to (ii). Furthermore, it was necessary to secure the numerical stability for each random realization (LHS simulation) of the input initial imperfections, which the application of (ii) did not fully ensure. The value of hardening slope, which is slightly greater than (ii) and provides sufficient numerical stability in each LHS simulation, was therefore numerically sought. The hardening slope of $E/10{,}000$ was used to overcome numerical instability, see Fig. 6. For short beams the numerically obtained values of $M_{LTB\text{-}R}$ based on $E/10{,}000$ are virtually identical with the control results that were calculated using the plateau slope of 1 MPa (ii). It can be noted that the stress-strain relationship can be introduced in other ways, see e.g. [37,3,38,34].

2.3. Geometric imperfections

Consideration of geometrical out-of-straightness imperfection in the analysis of structural behaviour is very important. The out-of-straightness imperfection was obtained by scaling the first eigenvalue LTB mode shape of a perfectly straight uniformly bending beam. The "scale factor" of e_0 was used to set the top flange maximum lateral imperfection at mid-span. The buckling mode was solved analytically as a pure elastic LTB problem; see e.g. [9,31,32]. The analytical solution very accurately matches the buckling mode obtained from the FE model. The advantage of the analytical solution is that the geometry in each LHS simulation can be quickly created automatically using the analytical formulas (1) and (2). Using the first eigenmode is very common in the investigation of the LTB phenomenon; see e.g. [4,39,6,40,41]. Both out-of-plane displacement v_0 and torsional imperfection φ_0 were included. These initial imperfections are affine to the deformed shape and can be described using the following sine functions:

$$v_0 = a_{v0}\sin\left(\frac{\pi x}{L}\right), \quad \varphi_0 = a_{\varphi_0}\sin\left(\frac{\pi x}{L}\right) \tag{1}$$

where v_0 is the curvature of the beam axis in the xy-plane and φ_0 is the rotation of the cross-sections along the beam length, see Fig. 7.

The following relationships are valid for amplitudes a_{v0} and $a_{\varphi 0}$ in a beam curved according to the first eigenmode

$$a_{v0} = \frac{|e_0|}{1+\frac{h}{2}\frac{\pi^2 EI_z}{M_{cr}L^2}}, \quad a_{\varphi_0} = a_{v_0}\frac{\pi^2 EI_z}{M_{cr}L^2} \tag{2}$$

where e_0 is the amplitude at midspan relating to the centre of the top edge of the flange, h is the cross-section height, I_z is the second moment of area to the z-axis, L is the length of the beam, E is Young's modulus of elasticity and M_{cr} is the elastic critical moment at lateral beam buckling, see e.g. [9,31,32].

It may be noted that the procedure for the polynomial approximation described in Chapter 5 requires 400 random realizations of the geometry of the imperfect beam I200 for each length L. The random characteristics of geometry are flange thickness t_2 and random amplitudes a_{v0} and $a_{\varphi 0}$ (1), the other geometric characteristics are deterministic. a_{v0} and $a_{\varphi 0}$ in (2) are randomly dependent on e_0, E, M_{cr}, I_z. M_{cr} is randomly dependent on t_2, E and I_z is randomly dependent on t_2 [32]. Thus, the geometry of the I-beam is randomly dependent on three input random variables e_0, t_2 and E.

2.4. Residual stress

Residual stress can play a significant role in evaluating the structural behaviour and is strongly dependent on the manufacturing process. Parabolic or linear distribution of residual stress on the web and flanges may be applied to I-sections [42]. The commonly used residual stress pattern for hot-rolled I-profiles in FE modelling is the linear stress distribution [43], see Fig. 8.

The magnitude and distribution of residual stress in hot-rolled shapes depend on the type of cross-section, rolling temperature, cooling conditions, straightening procedures, and the material properties of the steel [13]. An overview of approaches for the modelling of residual stress can be found, for e.g. in [3,34,44]. Results of numerical studies found in [33,45] tend to relate the values of the residual stress to the material yield strength of steel grade S235. For the ratio $h/b > 1.2$, which corresponds to I profiles, the mean value of the residual stress may be considered as 30% of

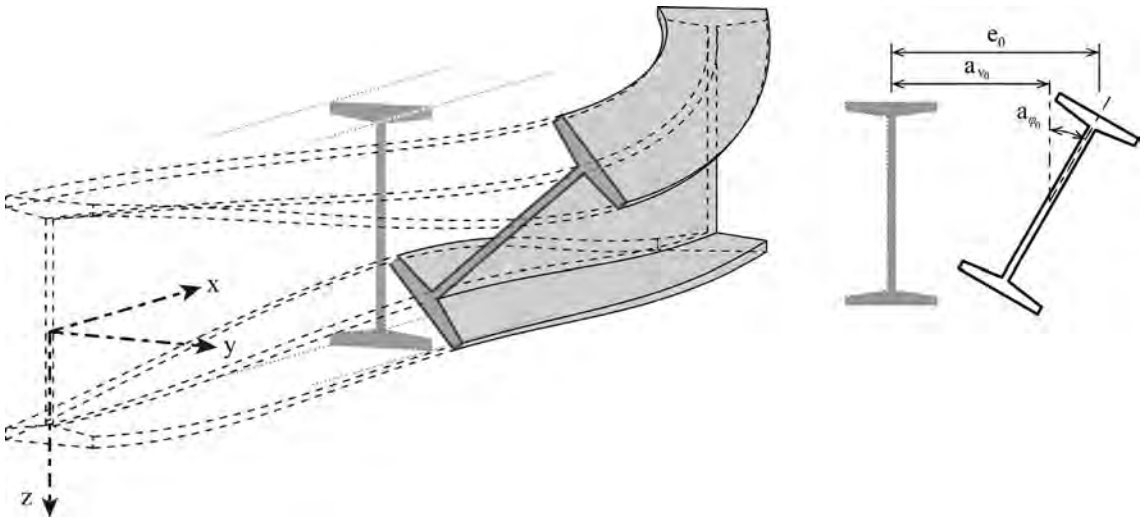

Fig. 7. Initial axis imperfection pattern based on the first mode of the elastic eigenvalue analysis.

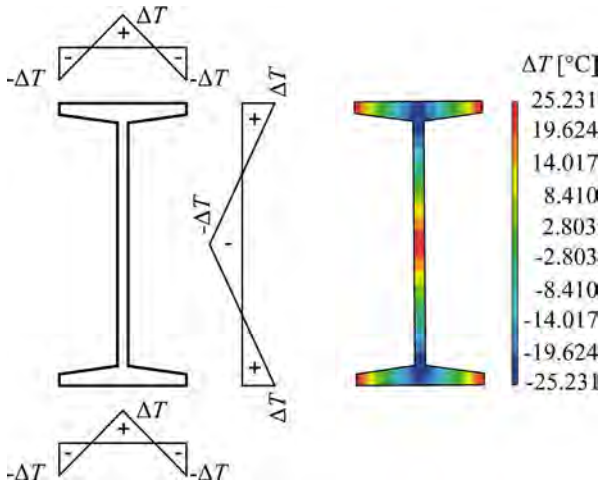

Fig. 8. Application of linear temperature changes ΔT for the initiation of residual stress.

the yield strength f_y, for ratio $h/b < 1.2$ (HE profiles) 50% of the yield strength is considered (for steel S235) [4,34]. Study [46] lists the values of residual stress at the flange edges of profiles IPE as 0.3×235 MPa independent of the yield strength for steel S235, S355 and S460. Measurements of the residual stress in flanges of similar shapes, made from different steel grades, show that the distribution and size of the residual stress are very similar [13]. Results of experimental research have shown that the size of residual stress in hot-rolled profiles seems to be independent of the material yield strength for both mild and high-strength steel [34].

Residual stress of the hot-rolled I200 beam was introduced in the form of self equilibrating stress distribution through initial thermal load step. Change in temperature ΔT at a point of the section is given by the formula

$$\Delta T = -\frac{\sigma_R}{E \cdot \alpha_t} \tag{3}$$

where σ_R is the residual stress in a given point and α_t is the thermal expansion coefficient, considered as $\alpha_t = 1.2\text{E}{-5}$ [K^{-1}]. Due to the overall configuration of the model the application of linear temperature change ΔT yields the desired stress σ_R only approximately. The precise (required) value σ_R is obtained by a new setting of ΔT, which is calculated by comparing the value attained (taken from the FE model) and the desired value of the residual stress when the dependency between σ_R and ΔT is linear. Boundary conditions of both ends of the column with the described kinematic constraints are implemented after the introduction of the residual stress. The distribution of longitudinal stress σ_x initiated by change in temperature ΔT is shown in Fig. 9. σ_R (blue)[1] is attained at the flange ends and in the centre of the web, whilst approximately $0.8 \cdot \sigma_R$ (red) is obtained in the flange-to-web connection, see Fig. 9. Lower stress $0.8 \cdot \sigma_R$ is due to the greater thickness of the flange in the flange-to-web connection, see Fig. 2. This difference does not occur in the case of beam models with rectangular flange shape (e.g. beams IPE, HEA, HEB), i.e. the absolute stress values from linear temperature change $\pm\Delta T$ are the same at the end and the middle of the flange.

3. Sobol sensitivity analysis

Sobol's method has the capability to perform SA for non-linear, non-additive and non-monotonic models. Let $Y = f(X_1, X_2, \ldots, X_N)$ be a deterministic model, where Y is a scalar output and X_i are N statistically independent input variables. The variance of Y can be decomposed into the form:

$$V(Y) = \sum_i V_i + \sum_i \sum_{j>i} V_{ij} + \sum_i \sum_{j>i} \sum_{k>j} V_{ijk} + \ldots + V_{123\ldots N} \tag{4}$$

where $V_i = V(E(Y|X_i))$ is the first order (main) partial variance and $V_{ij} = V(E(Y|X_i,X_j)) - V_i - V_j$ is the second order partial variance etc. V_i can be explained as the average reduction of model output variance resulting from fixing X_i, this means that V_i measures the individual contribution of X_i to the total variance $V(Y)$. The second order partial variance V_{ij} measures the second order interaction contribution between X_i and X_j to $V(Y)$). The higher order partial variances for quantifying higher order interaction contributions can be expressed analogously. By normalising the partial variances V_i, V_{ij}, V_{ijk} etc., according to the total variance $V(Y)$ we obtain Sobol sensitivity indices (5) of the first, second, third and higher orders.

$$S_i = \frac{V_i}{V(Y)}, S_{ij} = \frac{V_{ij}}{V(Y)}, S_{ijk} = \frac{V_{ijk}}{V(Y)}, \text{ etc.} \tag{5}$$

The total number of Sobol indices is $2^n - 1$. The sum of all Sobol indices must be equal to one.

$$\sum_i S_i + \sum_i \sum_{j>i} S_{ij} + \sum_i \sum_{j>i} \sum_{k>j} S_{ijk} + \ldots + S_{1,2,3\ldots N} = 1 \tag{6}$$

A more detailed description of Sobol's decomposition is in [25,26,22]. Examples of the application of SSA aimed at the stability and limit states of steel I-beams can be found in [32,47,48]. Although SSA is computationally demanding, it permits the exploration of all regions of the input space, accounting for interactions and non-linear responses.

4. Input random imperfections

The results of GSA [32] showed that LTB-E of an imperfect IPE-beam is most sensitive to the variability of four basic characteristics, namely yield strength (beams with low slenderness), Young's modulus (beams with high slenderness), flange thickness and the initial out-of-straightness of the beam axis. However, this conclusion was made on the basis of the analytical solution of LTB-E, in which the effects of residual stress were not modelled. Residual stress could be another significant imperfection if we were to study LTB-R.

The statistics of residual stress can be obtained from [49–51]. Three probability distribution models of residual stress evaluated from 103 measurements obtained from an extensive literature survey were defined in article [50]. Taking into account [50], we introduced two variants of the random variability of the residual stress. Residual stress at the flange edge is considered as input random variable rs. Gauss probability density function (pdf) with mean value $\mu_{rs2} = 90$ MPa and coefficient of variation 0.2 (standard deviation $\sigma_{rs2} = 18$ MPa) was considered in the variant rs_2. The residual stress is in the range of 10.5 MPa to 169.5 MPa if the LHS method is used to generate one hundred thousand numerical simulations. A four-parameter Hermite pdf [52] with $\mu_{rs1} = 90$ MPa, coefficient of variation 0.3 ($\sigma_{rs1} = 27$ MPa), skewness 0 and kurtosis 2.26 was considered in the variant rs_1. A residual stress range of 19.5–160.4 MPa was obtained from one hundred thousand numerical simulations generated using the LHS method, i.e. the observation interval is smaller than the Gauss pdf despite the larger standard deviation. Table 1 lists the comparison of statistical characteristics of variants rs_1 and rs_2 evaluated for 100 thousand LHS simulations. The comparison of both pdf types is presented in Fig. 10.

The statistical characteristics of yield strength of steel grade S235 were considered according to [53], where the results of

[1] For interpretation of color in Fig. 9, the reader is referred to the web version of this article.

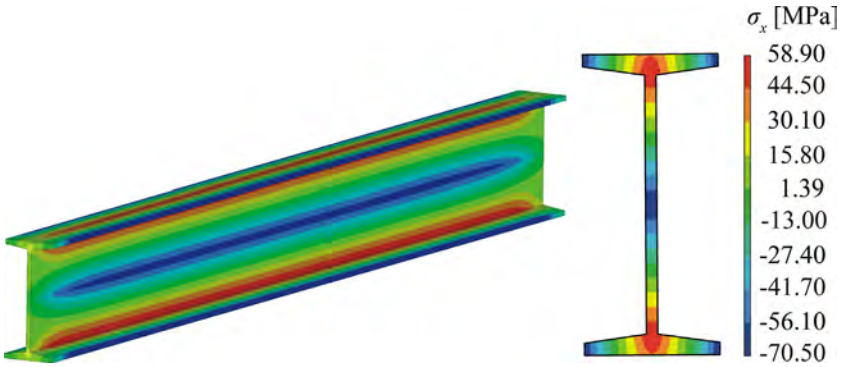

Fig. 9. Distribution of residual stress initiated by ΔT.

Table 1
Descriptive statistics of residual stress.

Variant names	rs_1	rs_2
Valid observations	100,000	100,000
Minimum	19.546	10.483
Maximum	160.45	169.52
Range	140.91	159.03
Median	90.000	90.000
Arithmetic mean	90.000	90.000
Geometric mean	85.452	88.094
Stand. deviation	27.259	18.000
Coef. of variation	0.3029	0.2000
Stand. skewness	−0.53E−08	−0.12E−12
Stand. kurtosis	2.2565	2.9995

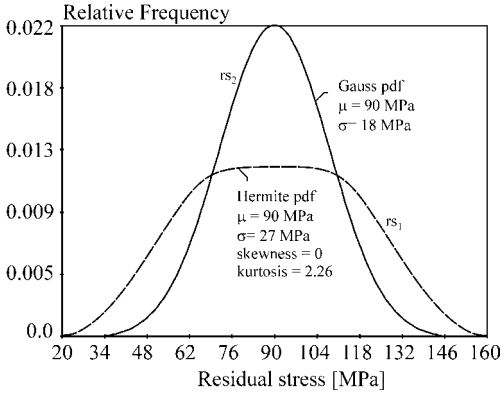

Fig. 10. The residual stress - Gauss and Hermite pdfs.

tensile tests of samples obtained from a third of flanges of profiles IPE 160 to IPE 220 were published. Note that the statistical evaluation of other independent experimental researches of the yield strength and other material characteristics of structural steel were published in [38,54]. The statistical characteristics of Young's modulus E were considered according to [55]. The statistical characteristics of flange thickness were considered according to [56].

The amplitude of initial imperfection e_0 (2) was considered as a Gauss pdf with mean value of zero $\mu_{e0} = 0$ (perfectly straight beam), which was taken from the JCSS Probabilistic Model Code [57,58]. Model Code [57] assumes that the pdf of e_0 is symmetrical around zero and that small eccentricities are more likely than large ones, although the large ones are more dangerous. The standard deviation of e_0 (σ_{e0}) was derived from the assumption that 95 observations (random realizations) of this imperfection are found in the tolerance limits [32]. The out-of-straightness tolerance can be considered in accordance with long-term experience as 0.1% L [59,4,39]. This is consistent with codes of practice regulating the acceptability of production tolerances of steel structures. However,

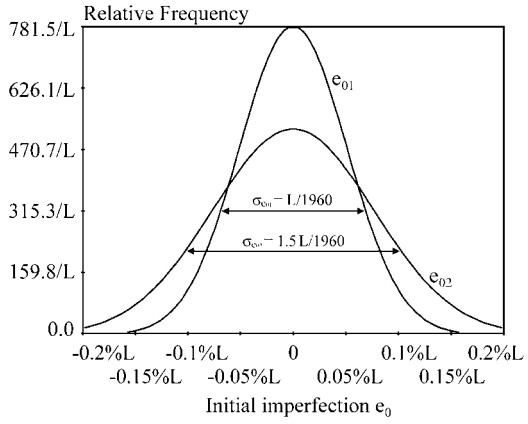

Fig. 11. The pdfs of initial imperfection e_0.

the straightness must comply with the requirements given in the European standard EN 10034:1993, which divides straightness tolerance q on length L into three groups according to height h [mm] for steel I and H sections: $80 < h < 180$, $q = 0.30\% L$; $180 < h < 360$, $q = 0.15\% L$; $h > 360$, $q = 0.1\% L$. The tolerance of hot-rolled section I200 is $q = 0.15\%$. Therefore two variants 0.1% L and 0.15% L of tolerance were considered. In summary, σ_{e0} was considered in two variants as $\sigma_{e01} = L/1960$ (0.1% L) [32,60] and $\sigma_{e02} = 1.5L/1960$ (0.15% L) [31], see Fig. 11. It may be noted that the Gauss pdf is not the only possible choice for e_0. For example [61] introduces a log-normal pdf for e_0 with $\mu_{e0} = L/3000$, $\sigma_{e0} = L/2551$ or $\mu_{e0} = L/2000$, $\sigma_{e0} = L/3785$. The use of the Hermite pdf [52] with a shape similar to rs_1 in Fig. 10, or a variant of the Hermite pdf with very small kurtosis that results in a "double-humped" and symmetrical around zero pdf may be discussed.

All input random geometric and material imperfections are listed in Table 2. Variables in Table 2 were considered as statistically independent. All other input geometric and material characteristics were considered using the nominal and characteristic (non-random) values of European standard I200 profile produced from steel of grade S235 [14], see Table 3.

5. Polynomial approximation of LTB-R

Sobol's method is much more computationally demanding in comparison to other global sensitivity analysis methods [21]. This is due to the fact that the series development of Eq. (6) has as many as $2^n - 1$ terms. One possibility to evaluate all $2^5 - 1 = 31$ Sobol indices is by approximating LTB-R using random realizations of the FE model output $M_{LTB\text{-}R}$. LTB-R is not calculated directly as $M_{LTB\text{-}R}$, but is represented by a polynomial (7) that has a quicker

response and which approximates all non-linear and interaction effects of non-linear FE model.

$$M_{\text{LTB-R}} \approx Y = \sum_{a=0}^{2}\sum_{b=0}^{2}\sum_{c=0}^{2}\sum_{d=0}^{2}\sum_{e=0}^{2} c_\alpha \cdot X_1^a \cdot X_2^b \cdot X_3^c \cdot X_4^d \cdot X_5^e \tag{7}$$

The terms of the polynomial consist of the products comprising of n-combinations (for $n = 0, 1, \ldots, 5$) from a set of ten elements consisting of variables X_1, X_2, X_3, X_4, X_5 and their squares, such that the exponent of each variable is at most two.

Approximation methods along with SA are not new and have been described, for e.g. with regards to the substitution of the limit state function using the Response Surface technique, which presents an acceptable compromise in terms of accuracy and computational effort, for the approximation of the limit state surface [62]. Polynomials suitable for the approximation of the limit state surface may contain non-linear terms, but usually do not retain the interaction effects of all higher orders. GSA and SSA generally require polynomials with more terms than approximations of the response surface type.

Polynomial (7) contains 5 input variables and has $3^5 = 243$ terms with constants c_α, where $\alpha = 0, 1, \ldots, 242$. Polynomials with $3^6 = 729$ terms for 6 input variables or polynomials with $3^7 = 2187$ terms for 7 input variables, etc., can be expressed similarly. Approximation of the model output using polynomial (7) is advantageous for the evaluation of large numbers of Monte Carlo (LHS) runs, especially for computational models with a small number of input random variables that require large computing effort for the evaluation of a simulation (one run).

Constants c_α were calculated using the least squares method. The LHS method was used to realize 400 simulations of random variables $X_1, X_2, \ldots, X_5$, listed in Table. 4, for which 400 runs of $M_{LTB\text{-}R}$ were then simulated. The variances of random variables listed in Table 4 are higher than the variances of random variables listed in Table 2, which allows approximation (7) based on Table 4 to use high numbers of LHS simulation of the random variables from Table 2. The domain of the approximation is defined by the minimum and maximum values of Rectangular pdfs in Table 4, which were obtained as the minimum and maximum values from 500 thousand simulations of random imperfections from Table 2. This means that polynomial (7) can be evaluated for up to 500 thousand LHS simulations of initial imperfections from Table 2.

6. Sensitivity analysis of LTB-R

The goal of SSA is to study the effects of the variabilities of initial imperfections from Table 2 on LTB-R. V_i was evaluated using ten thousand realizations of $E(Y|X_i)$. One realization of $E(Y|X_i)$ was performed by applying the approximation (7) and ten thousand LHS runs. The total variance $V(Y)$ was evaluated using (7) and 500 thousand LHS runs. All Sobol higher-order indices were evaluated in a similar manner. Overall, all thirty-one Sobol indices were evaluated.The SSA procedure can be described as follows: the non-dimensional slenderness of the beam $\overline{\lambda}_{LT}$ is selected (e.g. $\overline{\lambda}_{LT} = 0.9$) and the corresponding beam length is calculated L (e.g. $L = 2.5$ m). The relationship between L and $\overline{\lambda}_{LT}$ is listed in [14]. Lengths L are calculated according to the nominal parameters of an idealised cross-section, see Fig. 2. For I200 and $\overline{\lambda}_{LT} \leq 1.7$ it approximately holds that $L \approx 1.86\overline{\lambda}_{LT} + 0.41\overline{\lambda}_{LT}^2 + 0.71\overline{\lambda}_{LT}^3$, see Table 3. The analytical formula is given in [63]. The length L is an input parameter of the formulae of standard deviations in Tables 2 and 4. Realization of random variables in Tables 2 and 4 are simulated using the LHS method. Due to the beam symmetry, LTB-R is the same for plus or minus realization e_0, therefore realizations e_0 are considered using their absolute values in (2). The approximation polynomial (7) is compiled using Table 4. SSA of LTB-R is performed using (7) and Table 2.The variant of input imperfections with the probabilistic models corresponding closest to reality is t_2, f_y, E, e_{01}, rs_1, see Table 2. 31 Sobol indices are plotted in pie charts in Figs. 12–14, which clearly illustrate the changing effects of initial imperfections on LTB-R for three values of $\overline{\lambda}_{LT}$. The higher the value of Sobol's index, the higher the influence of the variability of initial imperfections on LTB-R. In order to obtain continuous curves of Sobol indices the step of 0.01 was considered for $\overline{\lambda}_{LT}$. First order sensitivity indices S_i are plotted in Fig. 15 and the crucial second order sensitivity indices S_{ij} are supplemented in Fig. 16. Similarly, S_i and S_{ij} for the other variants of initial imperfections from Table 2 are plotted; see Figs. 17–22. Sensitivity indices of the third and higher orders are relatively small. Thus, they are not plotted. It may be noted that the results in Figs. 17–22 do not depict the effects of variables h, b, t_1 because their random variabilities were neglected. This is in accordance with [32,35,64], where the small effect of the variability of variables h, b, t_1 on LTB-E and LTB-R was proven.

Table 3
Nominal geometric and material characteristics of I200.

Symbol	Characteristic	Value
h	Sectional height	200 mm
b	Sectional width	90 mm
t_1	Web thickness	7.5 mm
α	Inclination angle	14%
ν	Poisson's ration	0.3
G	Shear modulus	$E/(2(1+0.3))$
L	Beam length	$\approx 1.86\overline{\lambda}_{LT} + 0.41\overline{\lambda}_{LT}^2 + 0.71\overline{\lambda}_{LT}^3$

Table 4
Artificial random variables for approximation.

Symbol	Characteristic	Density	Minimum	Maximum
X_1	Flange thickness	Rectangular	8.83 mm	13.77 mm
X_2	Yield strength	Rectangular	217.43 MPa	377.17 MPa
X_3	Modulus of elasticity	Rectangular	162.46 GPa	257.54 GPa
X_4	Initial imperfection	Rectangular	−4.76 L/1960	4.76 L/1960
X_5	Residual stress	Rectangular	4 MPa	176 MPa

Table 2
Input random imperfections.

Symbol	Characteristic	Density	Mean μ	Standard deviation	Variant
t_2	Flange thickness	Gauss	11.3 mm	0.518 mm	t_2
f_y	Yield strength	Gauss	297.3 MPa	16.8 MPa	f_y
E	Modulus of elasticity	Gauss	210 GPa	10 GPa	E
e_0	Initial imperfection	Gauss	0	L/1960	e_{01}
		Gauss	0	1.5L/1960	e_{02}
rs	Residual stress	Hermite	90 MPa	27 MPa	rs_1
		Gauss	90 MPa	18 MPa	rs_2

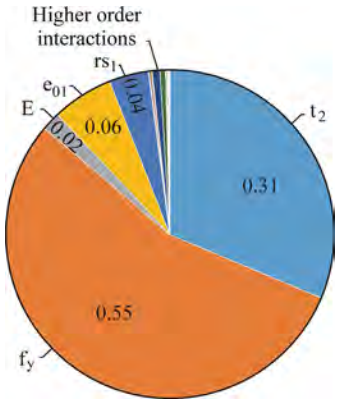

Fig. 12. SSA of LTB-R for variant t_2, f_y, E, e_{01}, rs_1 and $\bar{\lambda}_{LT} = 0.6$.

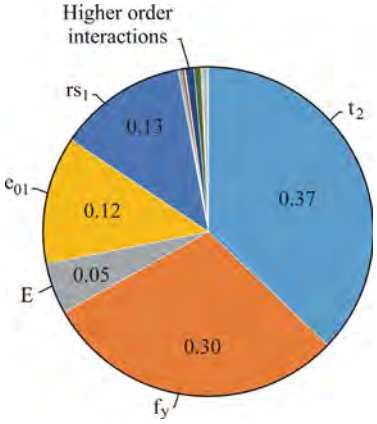

Fig. 13. SSA of LTB-R for variant t_2, f_y, E, e_{01}, rs_1 and $\bar{\lambda}_{LT} = 0.8$.

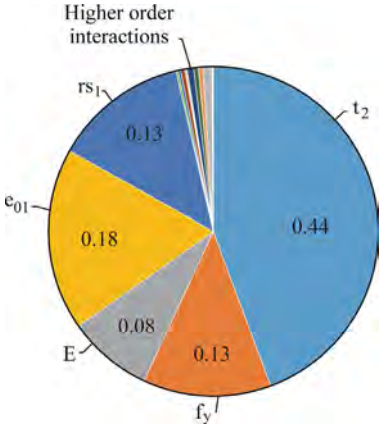

Fig. 14. SSA of LTB-R for variant t_2, f_y, E, e_{01}, rs_1 and $\bar{\lambda}_{LT} = 1.0$.

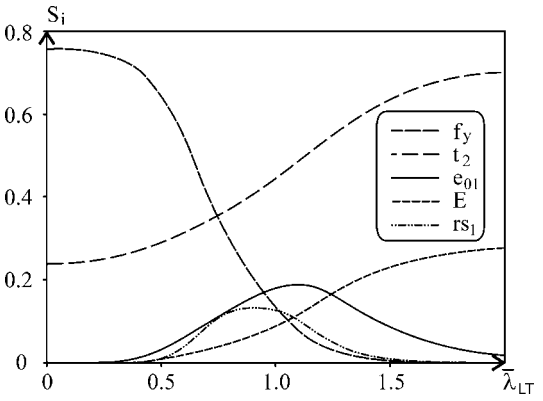

Fig. 15. First order indices S_i for variant t_2, f_y, E, e_{01}, rs_1.

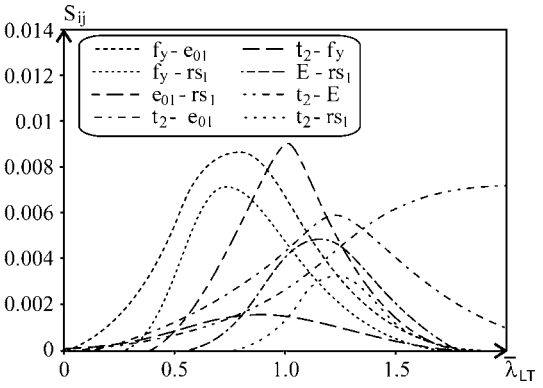

Fig. 16. Crucial second order indices S_{ij} for variant t_2, f_y, E, e_{01}, rs_1.

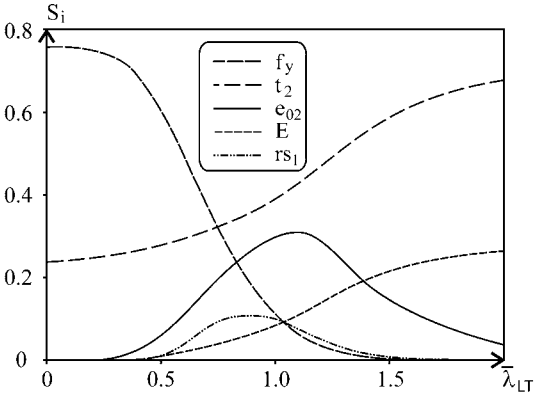

Fig. 17. First order indices S_i for variant t_2, f_y, E, e_{02}, rs_1.

The thick green curves are the SSA outputs of LTB-E. LTB-E is denoted in [32] as M_R (elastic load-carrying capacity) and is derived in the closed form. Let us note that the correctness of the analysis of M_R was verified using the geometrically non-linear FE model [63]. The analytical elastic solution M_R does not take into account the effect of residual stress. The input variables are otherwise the same for SSA, see Table 2.

Regarding the residual stress, the introduction of a high standard deviation σ_{rs1} = 27 MPa did not lead (as expected) to a high value of sensitivity index S_{rs1}, see Figs. 15 and 17. Sensitivity of LTB-R to rs_1 is relatively small. It is essential to properly understand this observation. SSA evaluates the effect of an imperfection while all other imperfections are varying as well. Whatever the strength interaction in the model, S_{rs1} indicates by how much one could, on an average, reduce the variance of LTB-R if rs_1 is fixed.Let us perform a comparison with deterministic study [65] investigating the effect of the inclusion or exclusion of the nominal value of residual stress on LTB-R of beam I200 with nominal imperfections. The residual stress reduced LTB-R by 6% for $\bar{\lambda}_{LT} = 1.2$, the effect was smaller for other values of slenderness.

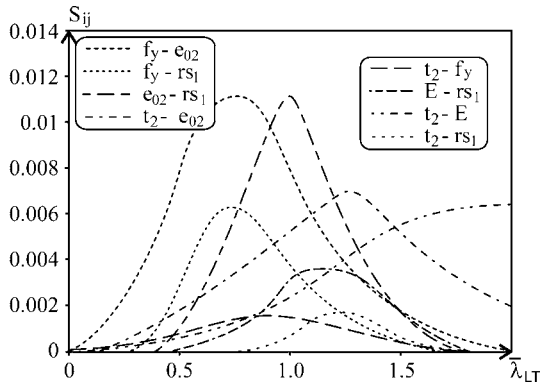

Fig. 18. Crucial second order indices S_{ij} for variant t_2, f_y, E, e_{02}, rs_1.

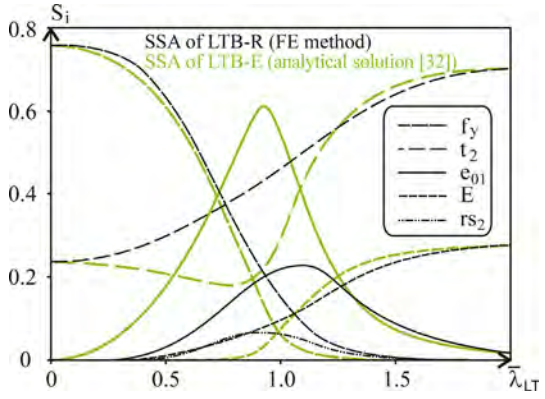

Fig. 19. First order indices S_i for variant t_2, f_y, E, e_{01}, rs_2.

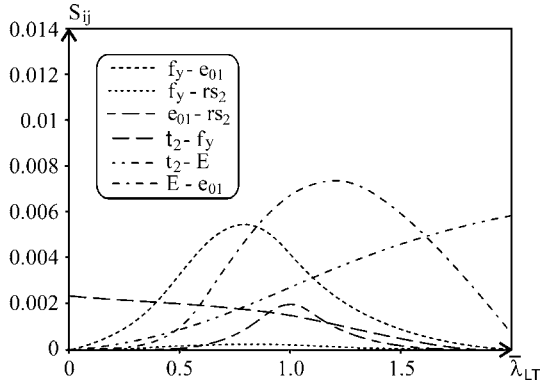

Fig. 20. Crucial second order indices S_i for variant t_2, f_y, E, e_{01}, rs_2.

This study belongs to the LSA category, because the value of the residual stress changes while all other imperfections are fixed. The effect of residual stress can generally be different if the other imperfections are set to different values. Using a two-valued change of another imperfection (e.g. e_0 as 0 and $L/1000$) can have a far greater effect on LTB-R than a two-valued change in residual stress. Changing the values of only some imperfections while keeping other imperfections fixed (no-change) can lead to the misinterpretation of their joint influence. Selection of the base case is very important in LSA. The SSA presented above provides much more information because it quantifies the overall contribution of each random input imperfection to the uncertainty of LTB-R.

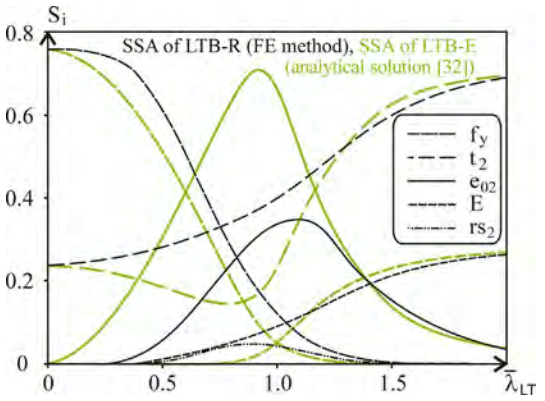

Fig. 21. First order indices S_i for variant t_2, f_y, E, e_{02}, rs_2.

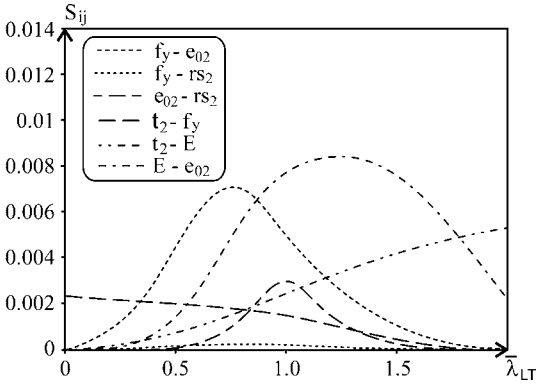

Fig. 22. Crucial second order indices S_i for variant t_2, f_y, E, e_{02}, rs_2.

7. Observations

The paper describes the detailed non-linear FE model and advanced numerical methods that were used for the in-depth sensitivity analysis of LTB-R. Table 2 lists the input random initial imperfections of the beam I200, for which SSA was performed. The results of SSA are useful for the comparison of the relative importance of the five initial imperfections, which are the model inputs of the LTB-R analysis. Unless stated otherwise, the conclusions of the SSA of LTB-R pertain to all solution variants; see Figs. 15–22.

- The influence of the residual stress rs_1 on LTB-R is relatively small despite the fact that random variable rs_1 was introduced with large variance. The same conclusion is true for random variable rs_2, which has lower (but also quite large) variance. The curves of sensitivity indices S_{rs1} and S_{rs2} reach their maximum for approximately $\bar{\lambda}_{LT} = 0.9$.
- Sensitivity index of yield strength S_{fy} has a plateau near $\bar{\lambda}_{LT} = 0$ and then decreases with increasing $\bar{\lambda}_{LT}$. For approximately $\bar{\lambda}_{LT} > 1.7$ $S_{fy} = 0$. This means that the variance of the yield strength can be fixed at any value of the domain without any effect on the variance of LTB-R.
- The influence of imperfection e_0 on LTB-R is the second dominant for $\bar{\lambda}_{LT} \approx 1.1$, especially for the variant e_{02}, which has 50% higher standard deviation than variant e_{01}. The curves of sensitivity indices S_{e01} and S_{e02} attain their maximum approximately for $\bar{\lambda}_{LT} = 1.1$. Sensitivity indices S_{e01} and S_{e02} are clearly higher than indices S_{rs1} and S_{rs2}.

- Sensitivity index S_{t2} of the flange thickness t_2 increases with increasing $\overline{\lambda}_{LT}$. t_2 is the absolutely dominant imperfection for $\overline{\lambda}_{LT} > 0.75$. This means that reducing the variance of t_2 has a relatively significant effect on the reduction of the variance of LTB-R. Reducing the variance of t_2 can be achieved by improving the production processes in metallurgical production.
- Sensitivity index of Young's modulus S_E increases with increasing $\overline{\lambda}_{LT}$. In contrast to t_2, the variance of E cannot be significantly influenced through technological processes in metallurgical production.

Second order sensitivity indices S_{ij} measure the second order interaction contribution between X_i and X_j to the variance of LTB-R. The values of S_{ij} shown in Figs. 16, 18, 20 and 22 are small, but provide interesting information on the non-linear response of an imperfect beam in limit state. Sensitivity to the yield strength f_y and the involvement of f_y in interactions determine, among other things, the sensitivity to plastic yielding. Plastic yielding does not occur when S_{fy} and fifteen additional higher-order indices involved in interactions with f_y are equal to zero. This is approximately fulfilled for $\overline{\lambda}_{LT} > 2.0$, otherwise at least one of the indices S_{fy}, $S_{t2,fy}$, $S_{fy,e0}$, $S_{fy,rs}$ always has a non-zero value.The relatively small values of all 26 higher-order sensitivity indices show that the non-linear model can be considered as approximately additive. This is favourable information for the selection of the approximation strategies that use second-order polynomials neglecting interaction effects. This conclusion applies to an individual beam; beams integrated into structural systems may be influenced by interactions with surrounding structures [66]. The thick green curves (Figs. 19 and 21) show the results of SSA of LTB-E, which were calculated using the elastic analytic solution in the closed form [31,32]. The thick green curves are very different in comparison with the black curves (SSA of LTB-R). The analytic elastic solution greatly exaggerates the importance of initial imperfections e_0 and on the contrary undervalues the importance of t_2 for the intermediate slenderness. This difference can be explained by the varied involvement of the flanges in the LTB-E and LTB-R solution. The thick green and black curves correspond for $\overline{\lambda}_{LT} = 0$ and $\overline{\lambda}_{LT}$= 2.0. The thick green curves of S_{e01} and S_{e02} are maximum for $\overline{\lambda}_{LT}$= 0.93 coinciding well with the maximum of S_{rs1} and S_{rs2}, which occurs in $\overline{\lambda}_{LT} = 0.9$. The thick green curves of S_{e01} and S_{e02} are also very similar in shape to the black curves of S_{rs1} and S_{rs2}. This is consistent with the frequently applied assumption that LTB-R taking into account the effect of residual stress can be approximately calculated as LTB-E of a beam with increased amplitude of initial imperfection e_0, sometimes referred to as the equivalent geometric imperfection.

8. Conclusion

GSA is an important part of the analysis of the reliability of steel structures and their limit states. SSA answers the question of which imperfections are dominant and should thus be paid increased attention during the preparation of the input values of stochastic models. Despite ongoing experimental research probabilistic models of initial curvature of the beam axis and residual stress are still under discussion. These imperfections influence the LTB-R, especially for I-beams with intermediate slenderness, which are commonly found in steel structures.

SSA showed that the random variability of residual stress *rs* has a smaller influence on LTB-R than the flange thickness t_2, axis curvature e_0 and yield strength f_y. Thus the statistical characteristics of residual stress need not be detected with such accuracy as t_2, e_0 and f_y. This conclusion is optimistic, because as we know, experimental research of residual stress is very difficult, time-consuming and an inefficient task with limited accuracy [44].

SSA showed that the random variability of e_0 has in some cases the second dominant effect on LTB-R. Thus the statistical characteristics and pdf type of e_0 must be determined with great accuracy, otherwise the results of probabilistic reliability analyses may be burdened with high error.The elastic solution LTB-E [31,32] overstates the influence of e_0, understates the importance of t_2 and does not take into account the effect of residual stress. For certain $\overline{\lambda}_{LT}$ the sensitivity of LTB-E to e_0 is more than twice higher than the sensitivity of LTB-R to e_0. Comparison of results of sensitivity analyses LTB-R and LTB-E can be useful for the probabilistic verification of stability design criteria of steel structures.

The results of SSA of LTB-R were obtained using the polynomial approximation of a FE model, which is a highly effective approach especially for numerically demanding models with a small number of input random variables. This approach made it possible to handle detailed numerical observation of the effects of imperfections on LTB-R, which could not otherwise be achieved.

Acknowledgements

This work was supported by project GAČR 14-17997S.

References

[1] Schillinger D. Stochastic FEM based stability analysis of I-Sections with random imperfections. Diploma thesis. Stuttgart University; 2008. p. 1–93.
[2] Vlasov VZ. Thin-walled elastic beams. Moscow; 1959.
[3] Boissonnade N, Somja H. Influence of imperfections in FEM modeling of lateral torsional buckling. In: Proceedings of the structural stability research council annual stability conference 2012. Elsevier; 2012. p. 399–413.
[4] Taras A, Greiner R. New design curves for lateral torsional buckling proposal based on a consistent derivation. J Constr Steel Res 2010;66(5):648–63.
[5] Schillinger D, Papadopoulos V, Bischoff M, Papadrakakis M. Buckling analysis of imperfect I-section beam-columns with stochastic shell finite elements. Comput Mech 2010;46(3):495–510.
[6] Agüero A, Pallarés FJ, Pallarés L. Equivalent geometric imperfection definition in steel structures sensitive to lateral torsional buckling due to bending moment. Eng Struct 2015;96:41–55.
[7] Zagari G, Zucco G, Madeo A, Ungureanu V, Zinno R, Dubina D. Evaluation of the erosion of critical buckling load of cold-formed steel members in compression based on Koiter asymptotic analysis. Thin-Walled Struct 2016;108:193–204.
[8] Giżejowski MA, Szczerba R, Gajewski MD, Stachura Z. Buckling resistance assessment of steel I-section beam-columns not susceptible to LT-buckling. Arch Civil Mech Eng 2017;17(2):205–21.
[9] Trahair NS. The behaviour and design of steel structures. New York: John Wiley & Sons; 1977.
[10] Timoshenko SP, Gere JM. Theory of elastic stability. 2nd ed. New York: McGraw-Hill; 1961.
[11] Bazant ZP, Cedolin L. Stability of structures elastic, inelastic fracture and damage theories. New York: Dover Publications; 1991.
[12] Chen WF, Atsuta T. Theory of beam-columns, vol. 1: in-plane behaviour and design, vol. 2, SPACE behaviour and design, McGraw-Hill, New York; 1977.
[13] Galambos TV. Guide to stability design criteria for metal structures. Structural Stability Research Council. 5thed. New York: John Wiley & Sons; 1998.
[14] EN 1993-1-1:2005 (E): Eurocode 3: design of steel structures-part 1-1: general rules and rules for buildings, CEN - European committee for Standardization, Brussels (Belgium); 2005.
[15] AISC LRFD American Institute of Steel Construction (AISC). Load and Resistance Factor Design, Chicago, AISC; 1994.
[16] BS 5950-1. Structural use of steelwork in building – Part 1: Code of practice for design – Rolled and welded sections. BSI; 2000.
[17] Mohri F, Damil N, Potier-Ferry M. Buckling and lateral buckling interaction in thin-walled beam-column elements with mono-symmetric cross sections. Appl Math Model 2013;37(5):3526–40.
[18] Borgonovo E, Plischke E. Sensitivity analysis: a review of recent advances. Eur J Oper Res 2016;248(3):869–87.
[19] Ferretti F, Saltelli A, Tarantola S. Trends in sensitivity analysis practice in the last decade. Sci Total Environ 2016;568:666–70.
[20] Wei P, Lu Z, Song J. Variable importance analysis: a comprehensive review. Reliab Eng Syst Safe 2015;142:399–432.
[21] Tian W. A review of sensitivity analysis methods in building energy analysis. Renew Sustain Energy Rev 2013;20:411–9.
[22] Saltelli A, Tarantola S, Campolongo F, Ratto M. Sensitivity analysis in practice: a guide to assessing scientific models. New York: John Wiley and Sons; 2004.
[23] Saltelli A, Ratto M, Andres T, Campolongo F, Cariboni J, Gatelli D, et al. Global sensitivity analysis—the primer. John Wiley and Sons, Ltd.; 2008.
[24] Annoni P, Bruggemann R, Saltelli A. Random and quasi-random designs in variance-based sensitivity analysis for partially ordered sets. Reliab. Eng. Syst. Safe. 2012;107:184–9.

[25] Sobol' IM. Sensitivity estimates for non-linear mathematical models. Math Model Comput Exp 1993;1(4):407–14. [Translated from Russian. Sobol', IM. Sensitivity estimates for nonlinear mathematical models. Matematicheskoe Modelirovanie 1990; 2(1):112–8].
[26] Sobol' IM. Global sensitivity indices for nonlinear mathematical models and their Monte Carlo estimates. Math Comput Simul 2001; 55(1–3): 271–80.
[27] Kala Z. Sensitivity assessment of steel members under compression. Eng Struct 2009;31(6):1344–8.
[28] McKey MD, Conover WJ, Beckman RJ. A comparison of the three methods of selecting values of input variables in the analysis of output from a computer code. Technometrics 1979;1(2):239–45.
[29] Iman RC, Conover WJ. Small sample sensitivity analysis techniques for computer models with an application to risk assessment. Commun Stat – Theory Methods 1980;9(17):1749–842.
[30] ANSYS Theory Release 15.1, ANSYS Inc.; 2014.
[31] Kala Z. Elastic lateral-torsional buckling of simply supported hot-rolled steel I-beams with random imperfections. Procedia Eng 2013;57:504–14.
[32] Kala Z. Sensitivity and reliability analyses of lateral-torsional buckling resistance of steel beams. Arch Civil Mech Eng 2015;15(4):1098–107.
[33] Kaim P. Spatial buckling behaviour of steel members under bending and axial compression. Ph.D. thesis. Technischen Universität Graz; 2004. p. 1–257.
[34] Jönsson J, Stan T-C. European column buckling curves and finite element modelling. J Constr Steel Res 2017;128:136–51.
[35] Valeš J. Sensitivity analysis of static resistance of slender beam under bending. AIP Conf Proc 2016;1738. 380008-1–380008-4.
[36] EN 1993-1-5:2006. Eurocode 3: design of steel structures – Part 1–5: plated structural elements. CEN - European committee for Standardization, Brussels, Belgium; 2006.
[37] Byfield MP, Davies JM, Dhanalakshmi M. Calculation of the strain hardening behaviour of steel structures based on mill tests. J Constr Steel Res 2005;61(2):133–50.
[38] Sadowski AJ, Rotter JM, Reinke T, Ummenhofer T. Statistical analysis of the material properties of selected structural carbon steels. Struct Saf 2015;53:26–35.
[39] Nguyen TT, Chan TM, Mottram JT. Influence of boundary conditions and geometric imperfections on lateral–torsional buckling resistance of a pultruded FRP I-beam by FEA. Compos Struct 2013;100:233–42.
[40] Ghafoori E, Motavalli M. Lateral-torsional buckling of steel I-beams retrofitted by bonded and un-bonded CFRP laminates with different pre-stress levels: experimental and numerical study. Constr Build Mater 2015;76:194–206.
[41] Panedpojaman P, Sae-Long W, Chub-uppakarn T. Cellular beam design for resistance to inelastic lateral – torsional buckling. Thin-Walled Struct 2016;99:182–94.
[42] Young BW. Residual stresses in hot rolled members. IABSE Rep Work Commiss 1975;23:25–38. http://dx.doi.org/10.5169/seals-19798.
[43] ECCS 1984. Ultimate limit state calculation of sway frames with rigid joints. ECCS Technical Committee 8 – Structural Stability: Technical Working Group 8.2 – System, European Convention for Constructional Steelwork. ECCS-Publication No. 33; 1984.
[44] Abambres M, Quach WM. Residual stresses in steel members: a review of available analytical expressions. Int J Struct Integr 2016;7(1):70–94.
[45] Taras A, Greiner R. Torsional and flexural torsional buckling—a study on laterally restrained I-sections. J Constr Steel Res 2008;64(7–8):725–31.
[46] Rebelo C, Lopes N, da Silva L Simões, Nethercot D, Vila Real PMM. Statistical evaluation of the lateral torsional buckling resistance of steel I-beams, Part 1: Variability of the Eurocode 3 resistance model. J Constr Steel Res 2009;65(4):818–31.
[47] Arwade SR, Moradi M, Louhghalam A. Variance decomposition and global sensitivity for structural systems. Eng Struct 2010;32(1):1–10.
[48] Kala Z. Global sensitivity analysis in stability problems of steel frame structures. J Civ Eng Manage 2016;22(3):417–24.
[49] Fukumoto Y, Itoh Y, Kubo M. Strength variation of laterally unsupported beams. J Struct Divis 1980;106(1):165–81.
[50] Shayan S, Rasmussen KJR, Zhang H. Probabilistic modelling of residual stress in advanced analysis of steel structures. J Constr Steel Res 2014;101:407–14.
[51] Zhang H, Shayan S, Rasmussen KJR, Ellingwood BR. System-based design of planar steel frames, I: reliability framework. J Constr Steel Res 2016;123:135–43.
[52] Kala Z. Global interval sensitivity analysis of Hermite probability density function percentiles. Int J Math Models Methods Appl Sci 2016;10:373–80.
[53] Melcher J, Kala Z, Holický M, Fajkus M, Rozlívka L. Design characteristics of structural steels based on statistical analysis of metallurgical products. J Constr Steel Res 2004;60(3–5):795–808.
[54] da Silva L Simões, Rebelo C, Nethercot D, Marquesa L, Simões R, Vila Real PMM. Statistical evaluation of the lateral-torsional buckling resistance of steel I-beams, Part 2: Variability of steel properties. J Constr Steel Res 2009;65(4):832–49.
[55] Soares GC. Uncertainty modelling in plate buckling. Struct Saf 1988;5(1):17–34.
[56] Kala Z, Melcher J, Puklický L. Material and geometrical characteristics of structural steels based on statistical analysis of metallurgical products. J Civ Eng Manage 2009;15(3):299–307.
[57] Model Code. Joint Committee of Structural Safety, JCSS; 2001. Available from: <http://www.jcss.ethz.ch>.
[58] Sedlacek G, Müller C. Zur Vereinheitlichung der Stabilitätsregeln im Eurocode 3 [Unified stability rules in Eurocode 3]. Stahlbau 2004;73(9):733–44.
[59] Aristizabal-Ochoa J Dario. Stability of multi-column systems with initial imperfections and non-linear connections. Int J Non-Linear Mech 2013;57:75–89.
[60] Kala Z. Reliability analysis of the lateral torsional buckling resistance and the ultimate limit state of steel beams with random imperfections. J Civ Eng Manage 2015;21(7):902–11.
[61] Sadovský Z, Nádaský P. Column strength curves in view of higher level reliability approach. In: Proceedings of the conference Eurosteel'99, ČVUT Praha; 1999. p. 125–8.
[62] Brenner ChE, Bucher Ch. A contribution to the SFE-based reliability assessment of nonlinear structures under dynamic loading. Probab Eng Mech 1995;10(4):265–73.
[63] Valeš J, Kala Z, Martinásek J, Omishore A. FE nonlinear analysis of lateral-torsional buckling resistance. Int J Mech 2016;10:235–41.
[64] Kala Z, Kala J. Sensitivity analysis of lateral buckling stability problems of hot-rolled steel beams. Slovak J Civ Eng 2009;2:9–14.
[65] Kala Z, Valeš J, Martinásek J. Inelastic finite element analysis of lateral buckling for beam structures. In: *CD proceedings of the 12th international conference modern building materials, structures and techniques*. Vilnius; 2016.
[66] Kala Z. Sensitivity analysis of steel plane frames with initial imperfections. Eng Struct 2011;33(8):2342–9.